REVISED LENS MODEL FOR THE MULTIPLY IMAGED LENSED SUPERNOVA, "SN REFSDAL" IN MACS J1149+2223*

KEREN SHARON AND TRACI L. JOHNSON
Department of Astronomy, University of Michigan, 1085 S. University Avenue,
Ann Arbor, MI 48109, USA; kerens@umich.edu

ABSTRACT

We present a revised lens model of MACS J1149+2223, in which the first resolved multiply imaged lensed supernova (SN) was discovered. The lens model is based on the model of Johnson et al. with some modifications. We include more lensing constraints from the host galaxy of the newly discovered SN, and increase the flexibility of the model in order to better reproduce the lensing signal in the vicinity of this galaxy. The revised model accurately reconstructs the positions of the lensed SN, provides magnifications, and predicts the time delay between the instances of the SN. Finally, we reconstruct the source image of the host galaxy, and position the SN on one of its spiral arms. Products of this lens model are available to the community through MAST.

Key words: galaxies: clusters: general – galaxies: clusters: individual (MACS J1149+2223) –
gravitational lensing: strong – supernovae: individual ("SN Refsdal")

1. INTRODUCTION

A discovery of a multiply imaged lensed supernova (SN) has always been considered a low-probability, high-gain possibility in SN surveys (e.g., Refsdal 1964; Kovner & Paczynski 1988), especially those focused on fields of lensing clusters. Although several lensed SN candidates have been reported (Goobar et al. 2009; Patel et al. 2014; Quimby et al. 2014), the recent discovery of a lensed SN in the field of MACS J1149+2223 (Kelly et al. 2014a, 2014b) is the first reported case of multiply imaged one, whose instances are detected and resolved.

"SN Refsdal" was discovered in *Hubble Space Telescope* (*HST*) WFC3/IR data obtained as part of the Grism Lens Amplified Survey from Space (GLASS; GO 13459, PI: Treu; Schmidt et al. 2014) between 2014 November 3 and 2014 November 20. We refer the reader to Kelly et al. (2014b) for details of the discovery. The host of "SN Refsdal" is a multiply imaged face-on spiral galaxy at $z = 1.491$, lensed by the cluster halo into three full images and one partial image (Smith et al. 2009), and further distorted by lensing perturbations by cluster galaxies. As we will show in the following sections, "SN Refsdal" occurred in one of the spiral arms of this galaxy, which happens to be going through secondary lensing by a cluster-member galaxy. The SN is thus lensed into four images around that cluster galaxy, in a configuration known as "Einstein Cross" (Kelly et al. 2014a).

MACS J1149+2223 is an X-ray bright, strong lensing cluster at $z = 0.543$ (Ebeling et al. 2007). Strong lensing models of MACS J1149+2223 were published by Smith et al. (2009) and Zitrin & Broadhurst (2009) based on shallow *HST* imaging (GO 9722; PI: Ebeling) and by Zitrin et al. (2011, 2014), and Rau et al. (2014) based on data from the Cluster Lensing and Supernova Survey with Hubble (CLASH) multicycle program (PI: Postman; Postman et al. 2012). Smith et al. (2009) also measured the spectroscopic redshifts of some of the lensed sources behind MACS J1149+2223. MACS J1149+2223 was

recently selected as one of the Hubble Frontier Fields (HFF; PI: Lotz) to be deeply imaged by *HST*. Preliminary lens models were derived by several teams prior to the deep HFF imaging, using a close to uniform set of constraints, but varying in lens modeling approaches, codes, and assumptions (PI: Sharon—Johnson et al. 2014; PIs: Kneib and Natarajan, CATS—Richard et al. 2014; PI: Bradač; PIs: Zitrin & Merten; PI: Williams). The results of these models were made available to the community through Mikulski Archive for Space Telescopes (MAST).[1] While these models provide a good description of the lens plane, they were not tailored to fit any one lensed source in particular, but to provide the best mass distribution and magnification estimates given a large set of constraints coming from lensed galaxies at different redshifts. This approach allows a better sampling of the slope of the mass distribution and facilitates studies of the magnified background universe.

In this Letter, we revise the model of Johnson et al. (2014, hereafter J14) and present a new lens model for MACS J1149 +2223, that better reproduces the lensing evidence at the vicinity of the multiply imaged lensed SN. We assume a flat cosmology with $\Omega_\Lambda = 0.7$, $\Omega_m = 0.3$, and $H_0 = 70$ km s^{-1} Mpc^{-1}. In this cosmology, $1''$ corresponds to 6.37 kpc at the cluster redshift, $z = 0.543$. Magnitudes are reported in the AB system.

2. LENS MODEL

We base our lensing analysis on the model presented by J14, with a few modifications, as described below. The model is computed with Lenstool (Jullo et al. 2007), using Markov Chain Monte Carlo (MCMC) sampling of the parameter space.

The positional constraints of the arcs lensed by MACS J1149 +2223 are identical to those in J14 (Figure 1), except for the main lensed source in this cluster, the face-on spiral galaxy at $z = 1.491$ that hosts "SN Refsdal." The constraints that we used in J14 did not favor this galaxy over other lensed sources, and used as lensing evidence only the brightest emission knot in each of the three full images of the source (1.1, 1.2, and 1.3

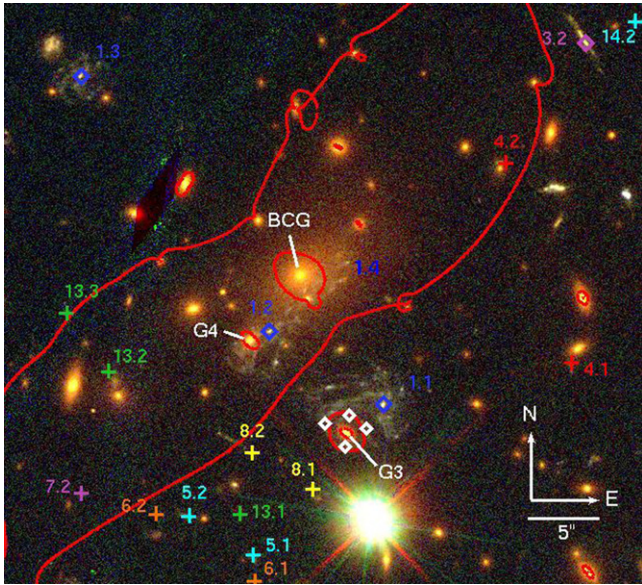[1] http://archive.stsci.edu/prepds/frontier/lensmodels/

Figure 1. Color composite image of the core of strong lensing cluster MACS J1149+2223 from *HST*/ACS F814W (red), F606W (green), and F435W (blue). The critical curves of the best-fit lens model are plotted in red for $z = 1.491$. The multiply imaged lensed sources that are used as constraints are color coded and labeled, with diamonds for sources with spectroscopic redshifts, and crosses for sources for which only photometric redshifts are available. For a full list of these images, including their coordinates, see J14. The three full images and fourth partial image of the host galaxy are labeled in blue, and the positions of the multiply imaged lensed SN are marked with white diamonds next to image 1.1. The constraints within the images of source 1 are shown in Figure 2

in Figures 1 and 2). Here, we take full advantage of morphological information and use as constraints several emission knots on the spiral arms of each of the lensed images of this galaxy. Figure 2 shows the lensing constraints that are used in this model.

The identification and mapping of the knots between the lensed images of this galaxy are aided by the lens model of J14, and constructed iteratively as higher levels of the current model were computed. Our identifications are done independently from those in Smith et al. (2009) and Rau et al. (2014), but are in general agreement with their identifications. With our final model, many more features can be identified (e.g., Rau et al. 2014); the features that are used as constraints here provide a uniform spatial coverage of the galaxy.

To the morphological constraints we add the positions of the four images of the SN from Kelly et al. (2014a), which appear around the cluster galaxy G3.

We note that the bright emission knot next to G4 is not used as a constraint in this model; the source reconstruction (see Section 3) supports the association of this knot, as well as other clumps East of G4, with secondary lensing by G4 that complicates image 1.2, as suggested by Zitrin & Broadhurst (2009) and Rau et al. (2014). However, since this knot is in close proximity to the critical curve of G4 we cannot determine whether it is indeed a counter image of the core of the lensed galaxy, or a different region that falls on the caustic and is therefore highly magnified. In total, there are three full images of the host galaxy, and additional images of some of the emission knots that form a partial forth image West of the brightest cluster galaxy (BCG), and a partial image near G4.

The mass distribution is composed of the five pseudo-isothermal elliptical mass distribution (PIEMD) halos in J14, with two additional halos that were individually optimized as described below. With the increased number of constraints around the images of source 1, we increase the flexibility of the model in these areas by freeing the parameters of the cluster galaxies closest in projection to 1.1 and 1.2. In particular, we allow the model to fit for the ellipticity, position angle, core and cut radii, and velocity dispersion of the galaxy that lenses the SN (G3), as well as the core, cut radii and velocity dispersion of the two central galaxies at the core of the cluster (BCG, G4). We also free some parameters that were fixed in J14 to be fitted by the model; however, we find that these parameters are consistent with the fixed values of J14.

Generally, each halo represents a sum of the mass distribution of the galaxy and the dark matter halo in which it is embedded, and the lens model does not distinguish between the two components. Thus, the best-fit parameters of some galaxy scale halos (e.g., G1) may seem higher than typical for galaxies.

Cluster galaxies are also included in the mass model as PIEMD halos, with parameters scaled with their luminosity. J14 used the cluster galaxies from Smith et al. (2009), selected from *K*-band imaging data. In order to increase the accuracy of the astrometric positioning of the cluster galaxies, we construct our galaxy catalog directly from the archival *HST* imaging, taken as part of the CLASH multicycle program (PI: Postman; Postman et al. 2012) and GO 9722 (PI: Ebeling; Smith et al. 2009). Cluster galaxies are selected from the *HST* ACS/ F606W and F814W photometry as those with F606W–F814W colors that place them on the cluster red sequence in a color–magnitude diagram. We assume $m_* = 20.04$ in ACS/F814W. The coordinates, ellipticity, and position angle of the cluster galaxies are fixed to their observed values, and the other parameters are scaled with their luminosity (see Limousin et al. 2005 for a description of the scaling relations). Our final model includes 116 constraints and 38 free parameters (Table 1). Among the constraints are three spectroscopic redshifts of lensed galaxies, measured by Smith et al. (2009). The redshifts of the other nine lensed galaxies are set as free parameters, with priors based on their photometric redshifts from Jouvel et al. (2013).

3. RESULTS AND CONCLUSIONS

Figure 1 shows the critical curves of the best-fit model over-plotted on a color image of the core of MACS J1149+2223. We find a significantly smaller scatter in the image plane for the lensed galaxy that hosts "SN Refsdal," with a typical scatter of $0\rlap{.}{''}15$ for individual emission knots. The image plane scatter of image 1.1 is reduced from $0\rlap{.}{''}83$ in J14 to $0\rlap{.}{''}03$ here. The lens model products are available to the community through the HFF modeling page on MAST.

We reconstruct the source-plane image of the host galaxy using methods described in Sharon et al. (2012, 2014), by ray-tracing the pixels of each image of the lensed galaxy to the source plane. As can be seen in Figure 3, the source reconstruction of images 1.1 and 1.3 is in excellent agreement. The north part of image 1.2 is also well matched to the other two images. The south part of this image, in particular the south spiral arm, is highly distorted in the lens plane by the cluster galaxy G4. Thus, the reconstruction of the
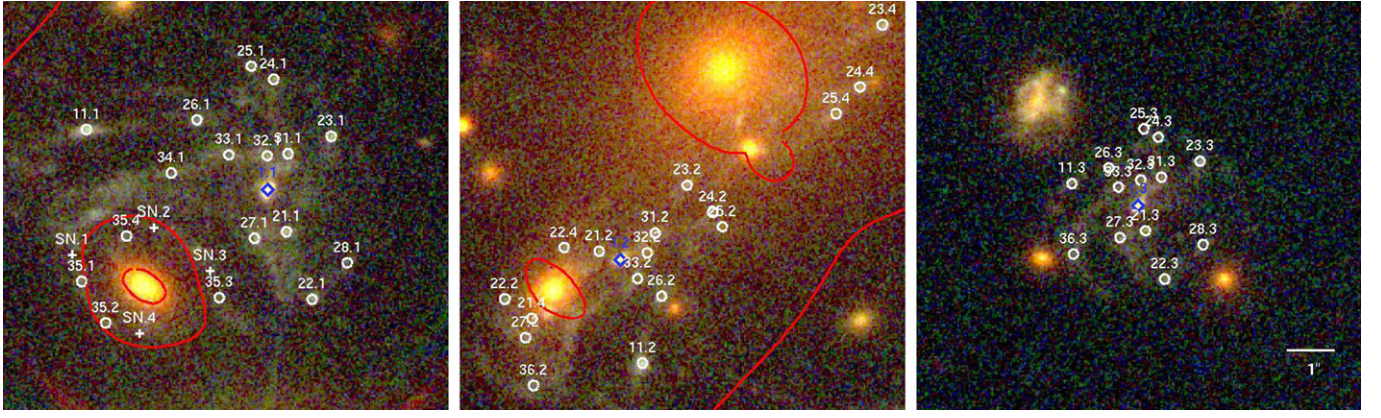
Figure 2. Zoom-in view on the three full images of the host galaxy; the emission knots that were used as constraints in this model are marked, as well as the SN positions from Kelly et al. (2014a).
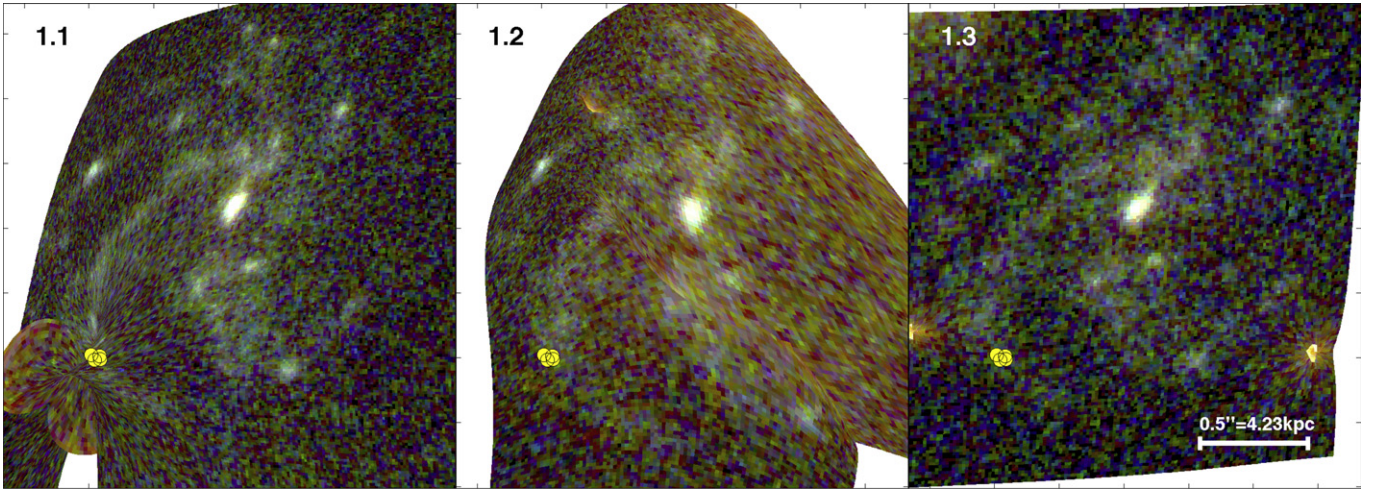

Figure 3. Source reconstructions from the three full images of the host galaxy are in excellent agreement. The positions of the SN images are ray-traced from image 1.1 to the source plane, and marked in yellow circles on all the source images, indicating that it most likely occurred in one of the spiral arms. Ghost-like features appear as a result of ray-tracing of light from the foreground galaxies.

Table 1
Best-fit Lens Model Parameters

Component	Δ R.A. ($''$)	Δ Decl. ($''$)	e	θ (deg)	r_{core} (kpc)	r_{cut} (kpc)	σ_0 (km s^{-1})
cluster halo 1 (H1)	$10.5^{+1.1}_{-1.4}$	$-6.85^{+1.21}_{-0.83}$	$0.61^{+0.01}_{-0.10}$	$23.8^{+4.8}_{-2.3}$	125^{+7}_{-15}	[1500]	914^{+69}_{-60}
cluster halo 2 (H2)	$-13.2^{+1.6}_{-1.4}$	$27.3^{+0.9}_{-4.4}$	$0.30^{+0.05}_{-0.14}$	$67.5^{+21.6}_{-5.5}$	[50]	[1500]	923^{+48}_{-79}
BCG (BCG)	[0]	[0]	$0.69^{+0.07}_{-0.10}$	$33.6^{+6.0}_{-0.1}$	$9.59^{+0.41}_{-2.19}$	[200]	416^{+17}_{-28}
cluster galaxy 1 (G1)	[25.6]	[−32.2]	[0.205]	[47.0]	[0.233]	[40.2]	527^{+31}_{-37}
cluster galaxy 2 (G2)	$17.0^{+0.0}_{-0.5}$	101 ± 1	[0.8]	$-54.4^{+1.0}_{-14.1}$	[0.261]	[300]	355^{+60}_{-2}
cluster galaxy 3 (G3)	[3.162]	[11.088]	$0.36^{+0.40}_{-0.17}$	$-34.2^{+2.9}_{-5.8}$	$0.16^{+2.93}_{-0.16}$	$3.60^{+1.09}_{-1.58}$	235^{+87}_{-11}
cluster galaxy 4 (G4)	[3.648]	[−4.568]	[0.355]	[48.3]	$1.34^{+1.29}_{-1.31}$	$3.67^{+7.36}_{-1.92}$	209 ± 67
L* galaxy	...	...	...	...	[0.15]	[30]	[150]

Notes. All the coordinates are measured in arcseconds east and north of the center of the BCG, at [R.A., Decl.] = [177.39875 22.398531]. Mass components are all PIEMD. The ellipticity of the projected mass density is expressed as $e = (a^2 - b^2)/(a^2 + b^2)$. θ is measured north of west. Error bars correspond to 1σ confidence level as inferred from the MCMC optimization. Values in square brackets are for fixed parameters that were not optimized. The location and the ellipticity of the matter clumps associated with the cluster galaxies were kept fixed according to their light distribution, and the other parameters were determined through scaling relations (see the text). Halo and galaxy notations are adopted from J14. G3 is the cluster galaxy closest to image 1.1, and G4 is the cluster galaxy closest to image 1.2.

south part of image 1.2 is not as well matched as it is in the other images. This may indicate that the modeling of G4 can be improved upon to better constrain the mass distribution of this galaxy.

We ray-trace the position of the SN through the best-fit lens model from the observed positions near G3, to the other images of the lensed galaxy. We find that the SN most likely occurred in one of the spiral arms of this galaxy (Figure 3). The source
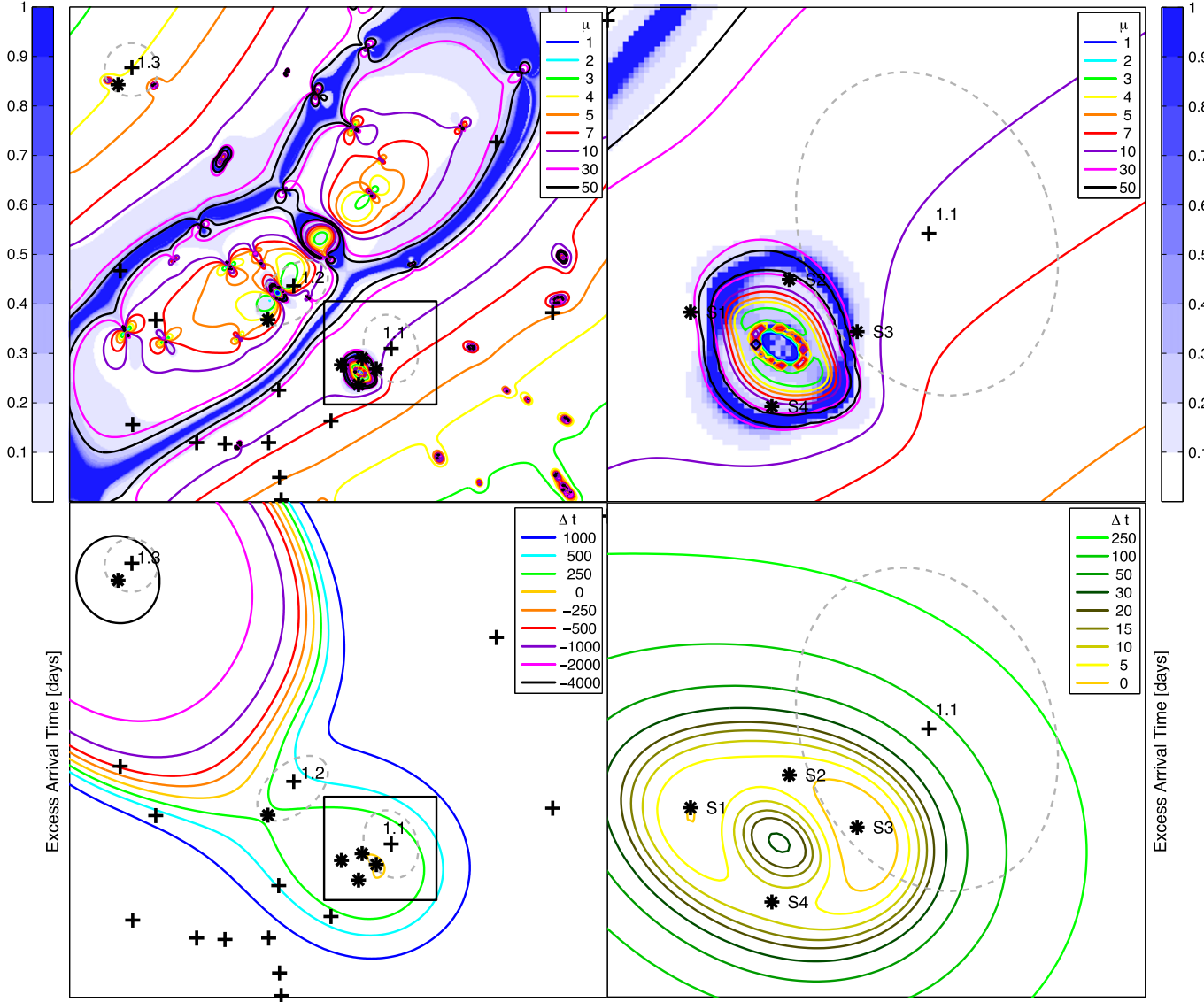
Figure 4. The top panels show the magnification and its uncertainty for a source at $z = 1.491$. The contours indicate the value of the magnification, and the color gradient indicates the uncertainty in the magnification in each position. The uncertainty is given in units of $\Delta\mu/\mu$. The field of view and scale are the same as those in Figures 1 and 2 for the left and right panels, respectively. To guide the eye, we plot the positions of the images of the lensed sources with black crosses, and the SN positions with black asterisks. The predicted SN images are also marked. The general extent of the host galaxy is indicated in dashed ellipses. The bottom panels show contours of the excess arrival time surface for light emitted from the source position in the source plane and traverses the lens plane. The excess arrival time is computed relative to S1 and given in days.

reconstruction is in good agreement with the results of Rau et al. (2014), who used a surface brightness distribution modeling approach.

Figure 4 maps the magnification (μ) and its fractional uncertainty ($\Delta\mu/\mu$) for a source at $z = 1.491$. We find a magnification of $\mu(1.1) = 10.2^{+0.5}_{-1.5}$ at the location of the brightest emission knot of image 1.1; at the location of the four images of the SN, the magnifications are somewhat higher, due to the added lensing boost from G3, $\mu(S1) = 18.5^{+6.4}_{-4.5}$, $\mu(S2) = 14.4^{+7.5}_{-5.5}$, $\mu(S3) = 20.5^{+19.1}_{-3.9}$, and $\mu(S4) = 11.0^{+6.9}_{-4.2}$, for images S1, S2, S3, and S4, respectively. Since the SN is practically a point source, microlensing by stars in the galaxy G3 (Schechter & Wambsganss 2002; Dobler and Keeton 2006), as well as millilensing by substructure with mass of order of star clusters (Mao & Schneider 1998; Metcalf & Madau 2001; Dalal & Kochanek 2002; Nierenberg et al. 2014),

may contribute to the magnification of some of the lensed images of the SN. This could affect the flux ratios between the SN images, and limit the use of flux ratios in modeling the system.

The arrival time surface for light emitted from the source location $\vec{\beta}$ and traverses a point $\vec{\theta}$ in the lens plane is given by (e.g., Schneider 1985)

$$\tau\left(\vec{\theta}, \vec{\beta}\right) = \frac{1 + z_l}{c} \frac{D_l D_s}{D_{ls}} \left[\frac{1}{2}\left(\vec{\theta} - \vec{\beta}\right)^2 - \psi\left(\vec{\theta}\right)\right], \quad (1)$$

where z_l is the lens redshift, D_l and D_s are the distances to the lens and the source, respectively, D_{ls} is the distance from the lens to the source, and ψ is the lensing potential. In the bottom panels of Figure 4 we plot the contours of the excess arrival time surface for light leaving the SN source position in the source plane, measured relative to the arrival time at the image-

plane location of S1, $\Delta t = \tau(\vec{\theta}, \vec{\beta}) - \tau(S1, \vec{\beta})$. Images occur at positions in the image plane in which the light travel time is stationary, i.e., minima, maxima and saddle points of this surface. Images S1, S3, and the predicted SN by 1.3 are minima, and images S2, S4, and the predicted SN by 1.2 are saddle points. The time delay predictions are given in days with respect to image S1 of the SN: $\Delta t_{S2-S1} = 2^{+10}_{-6}$, $\Delta t_{S3-S1} = -5^{+13}_{-7}$, $\Delta t_{S4-S1} = 7^{+16}_{-3}$ days. The time delay between S1 and the predicted location of the SN in the other lensed images of the host galaxy are of the order of years, with $\Delta t_{1.2-S1} = 237^{+37}_{-50}$ days, and $\Delta t_{1.3-S1} = -4251^{+369}_{-373}$ days. The local maximum near the center of G3 indicates that a demagnified SN image is predicted by the lens model, with a time delay of 36^{+12}_{-8} days and $\mu = 0.2 \pm 0.1$. The excess arrival time surface depends on the lensing potential and is highly sensitive to the inferred source plane position in this configuration. The source position is not an observed quantity, but is derived by the lens model in the modeling process. Each of the four images of the SN is ray-traced to a slightly different location in the source plane with a best-fit rms of $0\farcs02$. To estimate the uncertainties on the time delay, we therefore consider both the model uncertainties, by computing the potentials from models drawn from the MCMC parameter sets as above, and the scatter in the source position of the lensed SN. To account for this scatter, we compute 15 arrival time surfaces for each set of MCMC parameters, each with a source position that is a weighted-mean of the four computed SN source positions. The weights are set to either zero or one for each SN, and all the combinations are considered, thus sampling the area enclosed by the predicted source positions.

Our formal statistical uncertainties are drawn from a set of parameters that represent the lowest χ^2 steps in the chain that approximately span 1σ in the parameter space. Since the χ^2 estimator marginalizes over all the lensing constraints, some of these models result in a larger scatter in the source positions of the SN, balanced by lower scatter in other constraints. If we consider only the subset of models for which the SN source has a source plane scatter of $<0\farcs05$, the uncertainties are reduced by 30–60%: $\Delta t_{S2-S1} = 2^{+6}_{-4}$, $\Delta t_{S3-S1} = -5^{+7}_{-4}$, $\Delta t_{S4-S1} = 7^{+7}_{-3}$ days.

We find that the order of the arrival time is typically S3–S1–S2–S4, with 69% of the models predicting this order; 25% of the models predict arrival order of S1–S3–S2–S4. Most of the remaining models predict that S3 appears first. If considering only the models with low source-plane scatter, the order S3–S1–S2–S4 is predicted by 93% of the models.

We note that the lens model does not use time delays as constraints; at the time of this publication, time delays have not yet been measured. The relatively short time delays that are predicted by the lens model are consistent with the detection of three images of this SN at the same time.

A small part of the spiral arm in which the SN appears is lensed by the nearby cluster galaxy, G3, forming a ring around it. The archival data are not deep enough to uniquely identify substructure in this ring, but it will likely be feasible with the full depth of the HFF imaging. Nevertheless, the accurate positions of the newly discovered SN on this ring were used as constraints to model the mass distribution in this cluster galaxy;

we find that the galaxy is well described by a PIEMD halo centered on the observed light distribution (Table 1). We expect that the full depth of the HFF observation of MACS J1149+2223 will reveal ample new lensing constraints as new background sources are detected. These constraints will be most useful for reducing the uncertainties in the mass model of the cluster (e.g., Jauzac et al. 2014a, 2014b) and of the galaxy G3.

The discovery of a multiply imaged variable source with resolved images has interesting implications on constraining the mass distribution of its foreground lens. Follow up photometric observations of this source will reveal the time delay between the images, and measure their relative magnifications. Adding these unique SN constraints to the positional constraints can improve the lens model of G3 and the cluster in which it is embedded (e.g., Nordin et al. 2014). Such future analysis has the potential to constrain the truncation radius of the galaxy due to tidal stripping, measure the slope of its mass distribution, and the correlation between stellar mass and dark matter distributions, all of which can inform studies of galaxy evolution in cluster environment.

REFERENCES

Dalal, N., & Kochanek, C. S. 2002, ApJ, 572, 25
Dobler, G., & Keeton, C. R. 2006, ApJ, 653, 1391
Ebeling, H., Barrett, E., Donovan, D., et al. 2007, ApJL, 661, L33
Goobar, A., Paech, K., Stanishev, V., et al. 2009, A&A, 507, 71
Jauzac, M., Clément, B., Limousin, M., et al. 2014, MNRAS, 443, 1549
Jauzac, M., Richard, J., Jullo, E., et al. 2014, MNRAS, submitted (arXiv:1409.8663)
Johnson, T. L., Sharon, K., Bayliss, M. B., et al. 2014, ApJ, 797, 48
Jouvel, S., Host, O., Lahav, O., et al. 2013, yCat, 356, 29086
Jullo, E., Kneib, J.-P., Limousin, M., et al. 2007, NJPh, 9, 447
Kelly, P., Rodney, S., Treu, T., et al. 2014, ATel, 6729, 1
Kelly, P., Rodney, S., Treu, T., et al. 2014, arXiv:1411.6009
Kovner, I., & Paczynski, B. 1988, ApJL, 335, L9
Limousin, M., Kneib, J.-P., & Natarajan, P. 2005, MNRAS, 356, 309
Limousin, M., Kneib, J.-P., & Natarajan, P. 2001, ApJ, 563, 9
Mao, S., & Schneider, P. 1998, MNRAS, 295, 587
Metcalf, R. B., & Madau, P. 2001, ApJ, 563, 9
Nierenberg, A. M., Treu, T., Wright, S. A., Fassnacht, C. D., & Auger, M. W. 2014, MNRAS, 442, 2434
Nordin, J., Rubin, D., Richard, J., et al. 2014, MNRAS, 440, 2742
Ofek, E. O. 2014, Astrophysics Space Code Library, ascl:1407.005
Patel, B., McCully, C., Jha, S. W., et al. 2014, ApJ, 786, 9
Postman, M., Coe, D., Benítez, N., et al. 2012, ApJS, 199, 25
Quimby, R. M., Oguri, M., More, A., et al. 2014, Sci, 344, 396
Rau, S., Vegetti, S., & White, S. D. M. 2014, MNRAS, 443, 957
Refsdal, S. 1964, MNRAS, 128, 307
Richard, J., Jauzac, M., Limousin, M., et al. 2014, MNRAS, 444, 268
Schechter, P. L., & Wambsganss, J. 2002, ApJ, 580, 685
Schmidt, K. B., Treu, T., Brammer, G. B., et al. 2014, ApJL, 782, LL36
Schneider, P. 1985, A&A, 143, 413
Sharon, K., Gladders, M. D., Rigby, J. R., et al. 2012, ApJ, 746, 161
Sharon, K., Gladders, M. D., Rigby, J. R., et al. 2014, ApJ, 795, 50
Smith, G. P., Ebeling, H., Limousin, M., et al. 2009, ApJL, 707, L163
Zitrin, A., & Broadhurst, T. 2009, ApJL, 703, L132
Zitrin, A., Broadhurst, T., Barkana, R., Rephaeli, Y., & Benítez, N. 2011, MNRAS, 410, 1939
Zitrin, A., Fabris, A., Merten, J., et al. 2014, arXiv: 1411.1414